GEOPHYSICS, VOL. 57, NO. 1 (JANUARY 1992); P. 27–38, 8 FIGS.

Vector wavefields for weakly attenuating anisotropic media by the ray method

Dirk Gajewski* and Ivan Pšenčík‡

ABSTRACT

The ray method is used to compute high-frequency seismic vector wavefields in weakly attenuating layered anisotropic structures. The attenuating effects are introduced by substituting the real elastic parameters for perfectly elastic media by complex frequency dependent elastic parameters with small imaginary parts. The imaginary parts are formally considered to be of the order of ω^{-1} for $\omega \to \infty$. Under this assumption, it is possible to work with real rays, only the eikonal is complex. The approximate computations based on this algorithm are only a few percent slower than those for perfectly elastic anisotropic media. The range of applicability of the weak attenuation concept is investigated by comparison of ray computations with results of the reflectivity method for an isotropic, constant gradient model. The study indicates that the region of applicability of the weak attenuation concept may be broader than expected. The combined effects of anisotropy and attenuation on the propagation of seismic waves in a three-dimensional model of the uppermost crust with an anisotropic attenuating layer are then studied. The anisotropy as well as the attenuation are supposed to be caused by aligned partially liquid-filled cracks. Hudson's formulas to compute complex effective elastic parameters are used. Frequency responses and VSP synthetic seismograms for different degrees of viscosity of the liquid, and, thus, different degree of attenuation, show the effects of attenuation on the propagating waves. Nine-component VSP vector wavefields are computed for two different source-borehole directions along the strike of the cracks and 45 degrees off the strike of the cracks. The seismograms for the attenuating model are compared with seismograms for the corresponding perfectly elastic model.

INTRODUCTION

There is an increased interest in the investigation of wave propagation in fractured rocks, especially in rocks with aligned cracks (see numerous publications by Crampin and his coworkers, e.g., Crampin, 1985; 1987; 1990; Crampin et al, 1986; 1989). Fractured rocks with aligned cracks are effectively anisotropic. If the cracks are partially saturated with liquid, intrinsic attenuation occurs due to the energy losses by the fluid flow of the viscous fluid in cracks (see, e.g., O'Connell and Budiansky, 1977; Mavco and Nur, 1979; Hudson, 1988). The wavefield is also attenuated by scattering at cracks. This effect, however, is smaller than the effect of attenuation caused by partially saturated cracks, which dominates the total attenuation of fractured rocks (O'Connell and Budiansky, 1977). Here we do not distinguish between intrinsic attenuation and attenuation due to scattering and call the total effect attenuation. In anisotropic media attenuation generally depends on the wave-propagation direction.

The ray method is used to compute synthetic seismograms for weakly attenuating anisotropic structures, where the anisotropy and attenuation are caused by partially liquid saturated cracks. In the ray method for attenuating structures, complex rays must be considered. The assumption of weak attenuation allows us to work with real rays rather than complex rays, see Kravtsov and Orlov (1990). This considerably simplifies the computations. In this paper the ima-

Parts of this paper were presented during the 1989 SEG summer research workshop, "Recording and Processing Vector Wave Field Data." Manuscript received by the Editor January 18, 1991; revised manuscript received June 24, 1991.
*Formerly Center for Computational Seismology, Lawrence Berkeley Laboratory, Berkeley, CA; presently with Institute of Geophysics, Technical University of Clausthal, P.O. Box 1253, 3392 Clausthal-Zellerfeld, F. R. Germany.
‡Center for Computational Seismology, Lawrence Berkeley Laboratory, Berkeley, CA 94720; on leave from Geophysical Institute, Czechoslovak Academy of Sciences, Prague, Czechoslovakia.
© 1992 Society of Exploration Geophysicists. All rights reserved.

nary parts of the complex frequency-dependent elastic parameters are formally assumed to be of the order of ω^{-1} for $\omega \to \infty$, where ω is the circular frequency. The concept of weak attenuation has been applied to study attenuating laterally inhomogeneous isotropic media, for example, by Červený and Frangié (1982), Červený (1985), Červený and Pšenčík (1988), Moczo et al. (1987). Within this concept, noncausal as well as various causal attenuation models (see, e.g., Futterman, 1962; Kjartansson, 1979; Müller, 1983) can be considered. Attenuation effects on the reflection and transmission coefficients are not taken into account. The computations based on the weak attenuation concept are reasonably fast. For the examples presented in this paper, the CPU time requirements for computations in media with causal absorption are only slightly higher (by 10 percent) than for computations in perfectly elastic media.

The range of applicability of the described algorithm is tested by comparison of ray results with results of the reflectivity method (Fuchs and Müller, 1971; Sandmeier, 1984) for an isotropic, vertical gradient model. Synthetic vector wavefields are then computed for a three-dimensional (3-D) model containing isotropic and anisotropic attenuating layers. Both anisotropy and attenuation are caused by partially liquid-saturated aligned cracks. Frequency responses and vertical seismic profile (VSP) synthetics for different viscosities of the pore fluid are presented to show the effect of varying viscosities on the attenuation of the propagating waves. Nine-component VSP synthetics for two source-borehole azimuths running along the strike of the cracks and 45 degrees off strike are presented and compared with the seismograms for the corresponding perfectly elastic model.

WEAK ATTENUATION CONCEPT

In attenuating media, elastic parameters $c_{ijk\ell}$, as well as density-normalized elastic parameters $a_{ijk\ell}$ are complex-valued frequency dependent quantities

$$a_{ijk\ell}(\omega) = a^R_{ijk\ell}(\omega) - i a^I_{ijk\ell}(\omega). \tag{1}$$

Introduction of imaginary parts $a^I_{ijk\ell}$ leads, generally, to complications in ray computations. For example, instead of standard real rays, complex rays should be considered. If, however, absorption is only slight, such that $a^I_{ijk\ell} \ll a^R_{ijk\ell}$, the ray computation schemes for perfectly elastic media require only minor modifications to be approximately applicable to the attenuating media.

There are several possible ways of deriving the ray formulas for weakly attenuating media (Kravtsov and Orlov, 1990). In the procedure adopted here, the imaginary parts of parameters $a_{ijk\ell}$ are formally considered to be of the order of ω^{-1} for $\omega \to \infty$. Several authors have applied this procedure to weakly attenuating inhomogeneous isotropic media. If imaginary parts of elastic parameters $a^I_{ijk\ell}$ are considered as perturbations of $a^R_{ijk\ell}$, they produce perturbations of traveltimes only, see Moczo et al. (1987). We use this result as a starting point for derivation of ray formulas for weakly attenuating inhomogeneous anisotropic media to avoid lengthy derivations, similar to those made by the above-mentioned authors. In this way, the ray solution of the elastodynamic equation for a weakly attenuating medium can be written as

$$u_i(x_j, t) = U_i(x_j) \exp\{-i\omega[t - \tau^R(x_j) - i\tau^I(x_j)]\}. \tag{2}$$

Here $U_i(x_j)$ is the amplitude vector, τ^R is the traveltime of the considered wave. For details, see, e.g., Gajewski and Pšenčík (1987, 1990). The term $i\tau^I$ is the traveltime perturbation due to perturbations $ia^I_{ijk\ell}$ of parameters $a^R_{ijk\ell}$.

The perturbation method for anisotropic media (see, e.g., Jech and Pšenčík, 1989) provides the first order perturbation formula for $\tau^R + i\tau^I$,

$$\tau^R + i\tau^I = \int_{\tau_0}^{\tau} (1 + \tfrac{1}{2} i a^I_{ijk\ell}\, p_i p_\ell g_j g_k)\, d\tau^R, \tag{3}$$

where p_i are components of the slowness vector of the considered wave, $p_i = \partial\tau^R/\partial x_i$ and g_i are components of its unit polarization vector; τ_0 is the initial time of the ray and τ the arrival time. Note that (3) also follows from formula for real traveltime perturbations due to perturbations of the elastic parameters of an anisotropic medium, see Červený (1982), Hanyga (1982).

Let us denote by v the complex, frequency-dependent group velocity, $v(\omega) = v^R(\omega) - iv^I(\omega)$, with small imaginary part $v^I(\omega)$. Then we can express $\tau^R + i\tau^I$ also as follows,

$$\tau^R + i\tau^I = \int_{s(\tau_0)}^{s(\tau)} ds/v \approx \int_{s(\tau_0)}^{s(\tau)} \left(1 + i\frac{v^I}{v^R}\right)\frac{ds}{v^R}$$

$$= \int_{\tau_0}^{\tau} \left(1 + i\,\frac{v^I}{v^R}\right) d\tau^R \tag{4}$$

Comparing (3) and (4), we get, in first order approximation,

$$\frac{v^I}{v^R} = \tfrac{1}{2} a^I_{ijk\ell}\, p_i p_\ell g_j g_k. \tag{5}$$

Let us consider Futterman's relations,

$$\frac{i}{v(\omega)} = \frac{1}{v^R(\omega)}\left[1 + \frac{i}{2Q(\omega, p_n)}\right],$$

$$\frac{1}{v^R(\omega)} = \frac{1}{v^R(\omega_r)}\left[1 - \frac{1}{\pi Q(\omega_r, p_n)} \ln\frac{\omega}{\omega_r}\right], \tag{6}$$

$$Q(\omega, p_n) = Q(\omega_r, p_n)\left[1 - \frac{1}{\pi Q(\omega_r, p_n)} \ln\frac{\omega}{\omega_r}\right],$$

where ω_r is a reference frequency. From (5) and (6), we immediately get an expression for the quality factor Q in a weakly attenuating anisotropic medium

$$Q^{-1}(\omega, p_n) = a^I_{ijk\ell}(\omega)\, p_i p_\ell g_j g_k. \tag{7}$$

Thus, behavior of the quality factor is controlled by equation (7). The dependence of Q on slowness vector p_n expresses the dependence of the quality factor on the propagation direction of the considered wave. Note that for $a^I_{ijk\ell} = c a^R_{ijk\ell}$, where c is a small arbitrary real constant, the quality factor behaves isotropically since $a^R_{ijk\ell}$ satisfies the eikonal equation for perfectly elastic anisotropic media,

$$a^R_{ijk\ell}\, p_i p_\ell g_j g_k = 1, \tag{8}$$

and thus $Q^{-1}(\omega, p_n) = c$. The quality factor is, however, anisotropic in media effectively anisotropic due to aligned cracks. Corresponding complex elastic parameters for this case were derived by Hudson (1988). Applications based on Hudson's formulas are shown below.

We conclude this section with a final expression for the ray displacement vector of a wave propagating in a weakly attenuating inhomogeneous anisotropic medium:

$$u_i(x_j, t) = U_i(x_j) \times \exp\left\{-i\omega\left[t - \tau^R + \frac{t^*}{\pi}\ln\frac{\omega}{\omega_r}\right] - \tfrac{1}{2}\omega t^*\right\}, \quad (9)$$

where

$$t^* = 2\tau^I = \int_{\tau_0}^{\tau} a^I_{ijk\ell}\, p_i p_\ell g_j g_k \, d\tau^R \quad (10)$$

is the global absorption factor for an anisotropic medium. Equation (9) has exactly the same structure as for isotropic media, see Moczo et al. (1987). Therefore, the same numerical procedures as those described in the referenced paper can be used for the computation of synthetic seismograms. Equation (9) describes causal absorption; if the third term in brackets is omitted, equation (9) would describe noncausal absorption. According to equation (10) only a simple integration along the raypath is necessary to compute the attenuating effects in weakly attenuating anisotropic media.

APPLICABILITY OF THE WEAK ATTENUATION CONCEPT

The range of applicability of the weak attenuation concept is investigated by a comparison of ray synthetics with synthetic seismograms computed with the reflectivity method (Fuchs and Müller, 1971). For simplicity, an isotropic model is used for this purpose as the weak attenuation concept is based on the same assumptions in isotropic and in anisotropic media (small imaginary parts of complex elastic parameters, i.e., small imaginary parts of complex velocity in the isotropic case). For reflectivity computations a program written by Sandmeier (1984) is used. The ray computations are carried out with modified program package SEIS83 (Červený and Pšenčik, 1984).

A vertically inhomogeneous model with constant velocity gradient is used for the comparison. The model consists of a layer 2 km thick. The velocity at the surface is 4 km/s and 4.5 km/s at 2 km depth (a gradient of 0.25 s^{-1}). These velocities are specified for a reference frequency of 10 Hz. In the reflectivity computations, the velocity gradient was substituted by a stack of 0.01 km thick homogeneous layers (a total number of 200 layers). The layers were chosen so thin to obtain a good fit of traveltimes for reflectivity and ray computations. Larger layer thicknesses would result in increased traveltimes for the reflectivity method. The ratio of P-wave velocity to S-wave velocity v_P/v_S is $\sqrt{3}$ and the density is evaluated from the P-wave velocity using the relation $\rho = 0.2v_P + 1.7$. The P-wave and S-wave quality factors, Q_P and Q_S, are chosen constant throughout the layer and the same for both waves. They are successively infinite (i.e., the medium is perfectly elastic), 200, 50, and 30.

An explosive source located at 0.2 km depth is considered. A source-time function (see, e.g., Fuchs and Müller, 1971) with a prevailing period of 0.03 s (i.e., a prevailing frequency of 33 Hz) and 2 maxima is used. To satisfy the conditions of applicability of the ray method to the gradient model, the source time function is band-pass filtered. The filter equals unity between 6 and 95 Hz. Cosine smoothing is used between 5 and 6 Hz, and between 95 and 100 Hz. Outside this interval the filter is zero. The receivers are situated at the earth's surface.

Figure 1 shows the seismograms of the vertical component of the displacement vector of the refracted (diving) P-wave propagating in the perfectly elastic model. True amplitudes multiplied by a constant factor are shown. Figure 1a shows seismograms computed by the reflectivity method, Figure 1b shows seismograms obtained by the ray method. The perfect fit of seismograms in Figures 1a and 1b indicates that conditions of applicability of the ray method are satisfied. Figure 2 shows synthetics for the same model but with $Q = 200$. As in Figure 1, Figure 2a shows seismograms computed by the reflectivity method, Figure 2b by the ray method. The

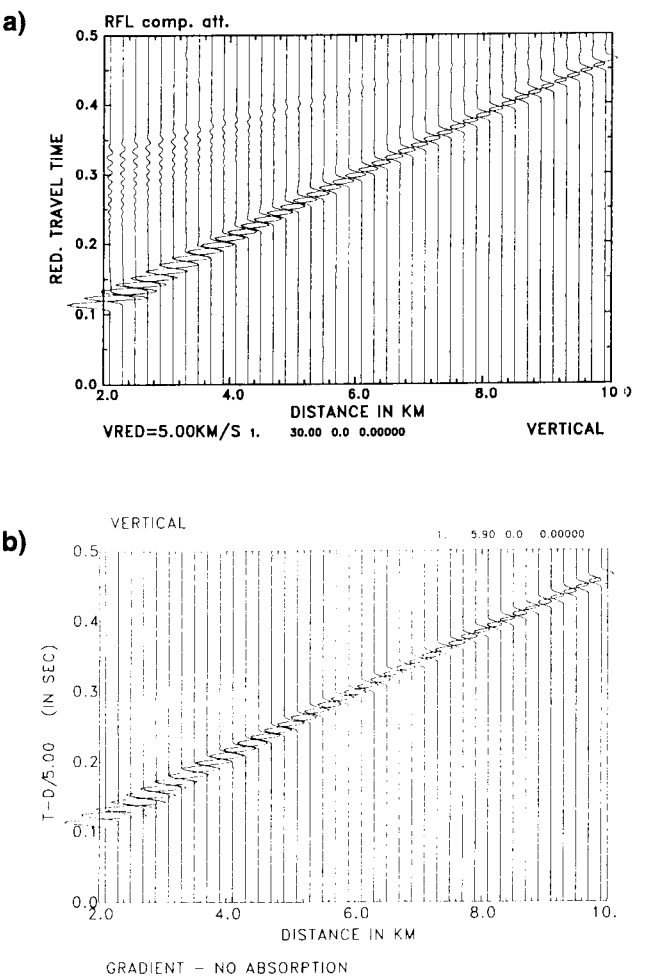

FIG. 1. Synthetic seismograms of the refracted P-wave for a vertically inhomogeneous isotropic perfectly elastic model calculated with (a) the reflectivity method and (b) the ray method.

same scaling of amplitudes as in Figure 1 is used. The results obtained by both methods are practically identical for this value of Q. Note that amplitudes for receivers with largest offsets are less than half the corresponding amplitudes for the perfectly elastic model. Also note the differences in waveforms between Figures 1 and 2.

Figure 3 shows synthetic seismograms for the same model, but with $Q = 50$. Even in this case a good fit of ray and reflectivity results is obtained. The ray seismograms have a sharper onset indicating higher high-frequency content than in the corresponding reflectivity seismograms. This means that the weak absorption concept reaches for this value of Q the limit of its applicability. Due to the low Q value, strong dispersion is observed in the synthetic seismograms. The amplitudes for the model with $Q = 50$ are a third of those for the perfectly elastic medium even for receivers with the smallest offset.

Further decrease of the Q value leads to more pronounced differences between ray and reflectivity results. Ray method signals are stronger and have higher high-frequency content than those computed by the reflectivity method.

In Figure 4, we show frequency responses (upper line), amplitude spectra of the seismograms (middle line), and synthetic seismograms obtained by ray computations for the receiver at $x = 4.3$ km. The columns from the left to the right correspond successively to the perfectly elastic model, and the attenuating models with $Q = 200$, 50, and, for comparison, $Q = 30$ (remember that for $Q = 30$, the ray method results differ from the reflectivity results). We can see an expressive reduction of the width of the amplitude spectrum and a shift of the frequency maximum towards lower frequencies with decreasing values of Q. The relative width, i.e., the width of the spectrum at half of the spectral maximum divided by the frequency of the spectral maximum, remains, however, nearly constant. A substantial reduction in the amplitude of the spectral maximum (see the values of reduction factors above upper right corners of frames) is observed. We can see that for $Q = 50$ the spectral maximum is 4 times lower than for a perfectly elastic medium. Comparing synthetic seismograms, we can observe broadening of signals caused by increasing dispersion with decreasing Q. High frequencies form the beginning of the signal, while the end of the signal has more low-frequency content. Note that with decreasing value of Q, the first arrival shifts to earlier arrival times. This phenomenon is caused by the lower value of the reference frequency (10 Hz), for which the velocity distribution is specified, than is the prevailing frequency of signal in perfectly elastic medium.

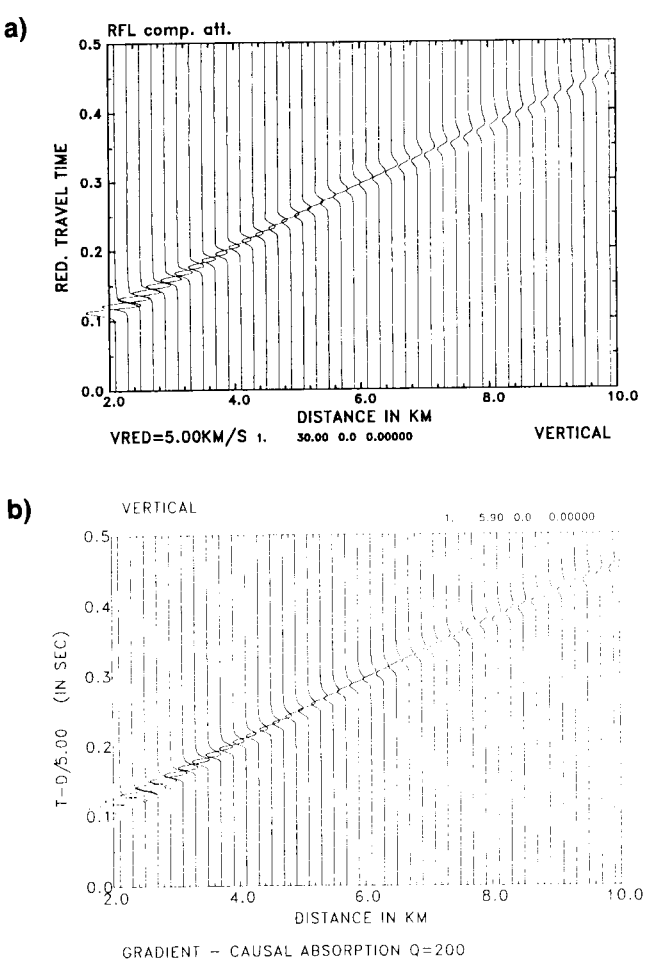

FIG. 2. The same as Figure 1 but for the attenuating model with $Q = 200$.

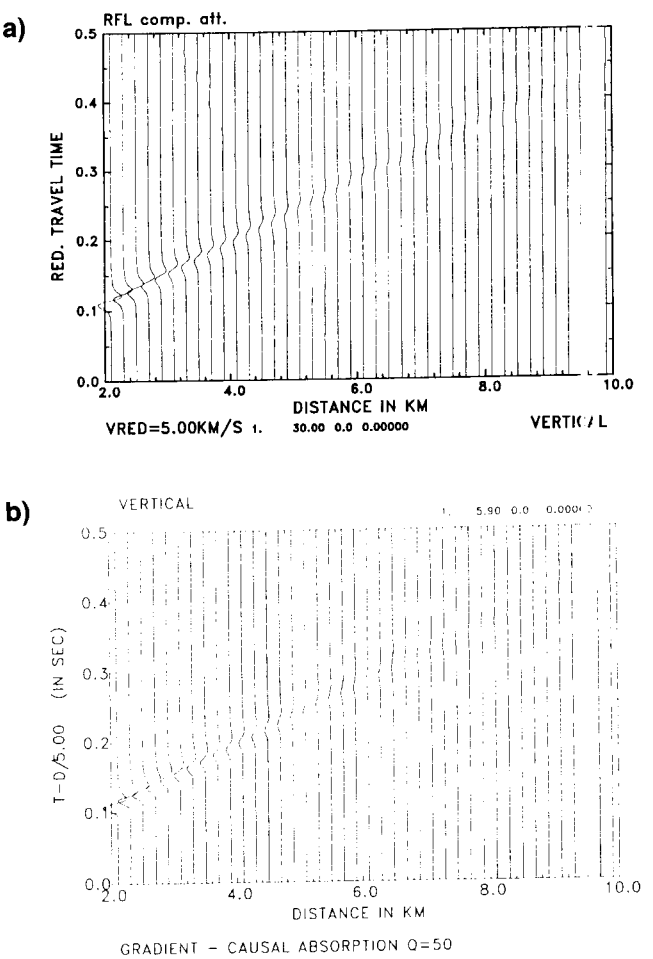

FIG. 3. The same as Figure 1 but for the attenuating model with $Q = 50$.

The comparison shown in this section demonstrates that the weak absorption concept can be applied to a substantial range of Q values encountered in exploration seismics. The value $Q = 50$ (limit where both reflectivity and ray method give almost identical results) corresponds to imaginary parts of complex group velocity which are 100 times smaller than real parts. Therefore, we take the condition that imaginary parts of complex group velocity must be more than 100 times smaller than real parts or the condition that the computed values of Q must be larger than 50 as a rough criterion of the applicability of the weak attenuation concept. These conditions can be checked at each point of a considered ray.

NUMERICAL EXAMPLES

In this section we present results compared for a 3-D upper crust model containing isotropic and anisotropic attenuating layers. The weak attenuation concept described above was incorporated into the program package SEISAN88, see Gajewski and Pšenčík (1987; 1990). For the computation of the global absorption factor for anisotropic layers, equation (10) is used. For isotropic layers this equation reduces to that given by Moczo et al. (1987). Causal absorption is considered in all computations. For the computations of synthetic seismograms, the spectral approach including a fast frequency algorithm suggested by Červený (1985) was used. At each receiver, the frequency response was computed for frequencies from 0.5 to 100 Hz with a step of 0.5 Hz. The response for a receiver and a specified frequency is determined as a sum of contributions of rays corresponding to the considered waves terminating at the receiver. Once the frequency response is known, the amplitude spectrum for a seismogram is obtained by multiplication of the frequency response with the filtered spectrum of the signal. Finally a FFT is applied to construct synthetic seismograms.

Model, sources, receivers and considered waves

Let us consider a Cartesian coordinate system with the x and y axes horizontal and the z-axis vertical, positive downward. The positive orientation of the x-axis is to the east, of the y-axis to the south, so that the system is right-handed. The model itself is situated in a cube. Its northwest upper corner coincides with the origin of the Cartesian coordinate system. The length of an edge of the cube is 5 km. The top side of the cube represents the free surface, the bottom side the bottom of the model. Vertical sides of the cube form vertical boundaries of the model.

The model consists of three homogeneous layers separated and/or limited by four interfaces. In Figure 5, a schematic 3-D image of the model is shown. With respect to the geometry of the interfaces, the model is axially symmetric with a vertical symmetry axis through $x = 2.5$, $y = 2.5$ km. Interface 1 is a flat horizontal boundary, and represents the free surface, situated at $z = 0$ km. Interface 2, forming

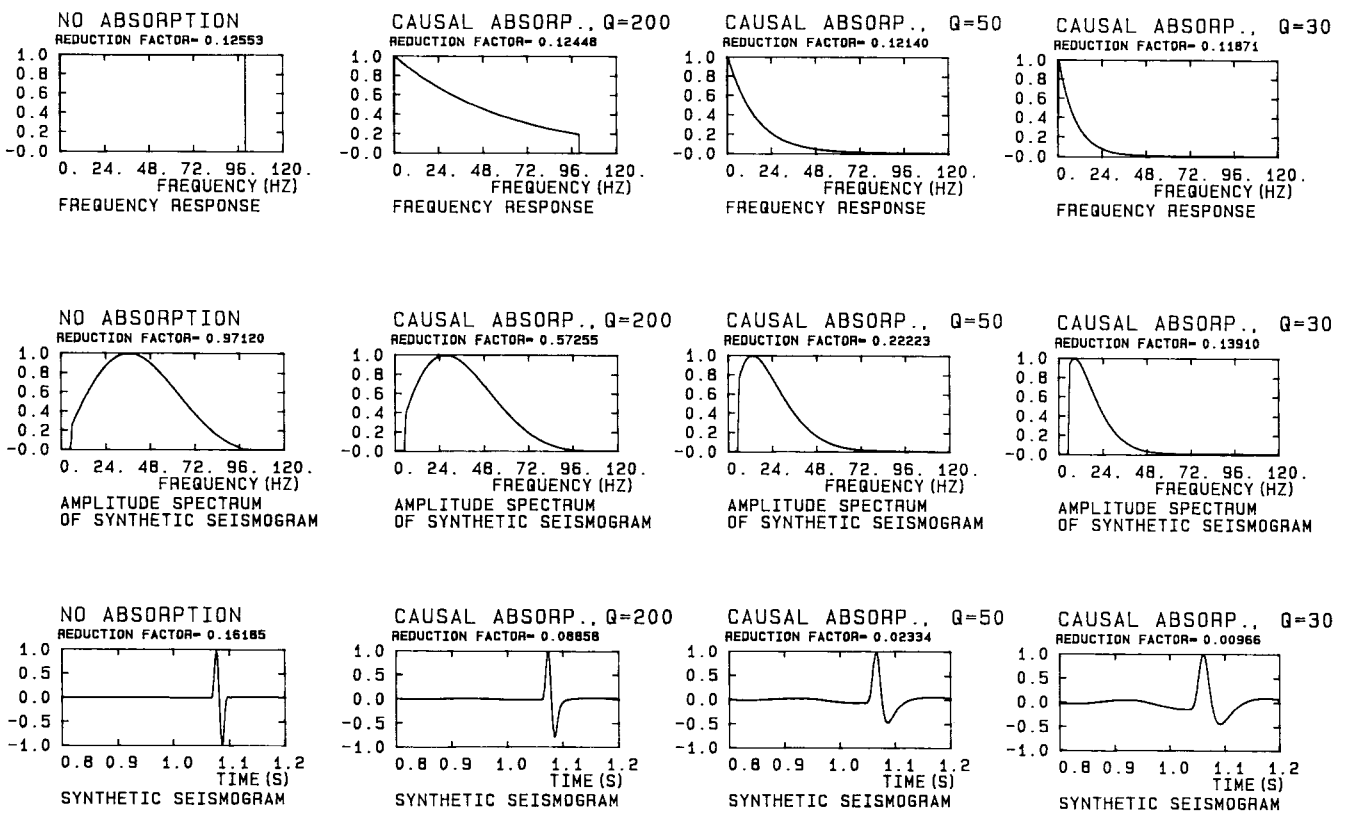

FIG. 4. Frequency responses (top), amplitude spectra of seismograms (middle) and synthetic seismograms of the vertical component of the displacement vector generated by an explosion and recorded at the receiver at $x = 4.3$ km. From left to right: perfectly elastic model, attenuating models with $Q = 200$, $Q = 50$, and $Q = 30$.

the bottom of layer 1, is also flat and horizontal. It is situated at $z = 0.4$ km depth. Interface 3 has a trough-shaped form with the deepest point at $x = 2.5$, $y = 2.5$ km, and a depth of $z = 2.0$ km. The interface intersects the vertical boundaries of the model along horizontal lines at a depth of $z = 1.0$ km. Flat and horizontal interface 4, situated at the depth of 5 km represents the bottom of the model.

Elastic parameters inside layers are constant. The first and third layers are isotropic and perfectly elastic with P-wave velocities equal to 2.5 and 4.5 km/s and S-wave velocities equal to 1.44 km/s and 2.59 km/s, respectively. The second layer is assumed to be formed by aligned, partially liquid saturated cracks (70-percent saturation) in an isotropic host rock. Partial liquid saturation of cracks produces higher attenuation than 100-percent saturated cracks, see, e.g., laboratory results of Mavco and Nur (1979). The crack density is 0.1 and the aspect ratio is 10^{-3}. The crack radius is assumed to be 10^{-4}m (micro cracks). The strike of the cracks is along the north-south direction, i.e., along the y axis, and the dip is 70 degrees, with cracks dipping towards the west. The P-wave velocity of the host rock is 3.0 km/s and the v_P/v_S ratio is 1.783. Such a composition makes the layer effectively anisotropic with hexagonal symmetry and attenuating (Hudson, 1981; Crampin, 1984; Hudson, 1988). The axis of symmetry is located in the x, z plane and deviates from the horizontal plane by 20 degrees. The resulting complex density-normalized elastic parameters were obtained from Hudson's (1981, 1988) formulas. The velocity anisotropy of partially liquid saturated cracks does not depend on the degree of saturation and equals the velocity anisotropy of dry cracks.

The elastic parameters are specified in the coordinate system associated with the crystal axes and the symmetry axis is considered as the x-axis in the crystal coordinate system. The dimension of the complex density-normalized elastic parameters is $(km/s)^2$; compressed notation is used. For each elastic parameter, two values in brackets are given.

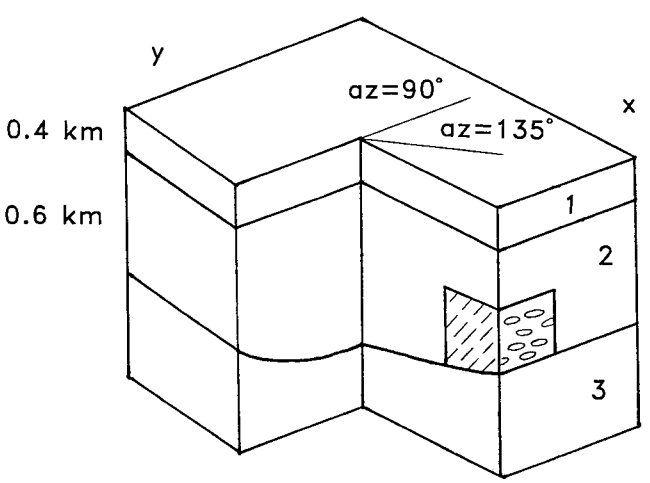

FIG. 5. Scheme of VSP experiment. The strike of the cracks is along the y-axis. The dip of the cracks is 70 degrees. The lines connecting two source locations to the mouth of the borehole are two considered profiles with azimuths of 90 degrees, and 135 degrees, respectively (azimuth measured from x-axis).

The first is the real part of the complex elastic parameter and the second is its imaginary part. For partially liquid-saturated cracks only A_{11}, A_{22}, and A_{12} have nonzero imaginary parts. The following values were obtained for harmonic waves with a frequency of 50 Hz (this frequency serves as reference frequency in the causal absorption computations). Three different values of kinematic viscosity (i.e., viscosity divided by the density of the liquid) are considered. The degree of saturation is kept constant (70 percent). For a kinematic viscosity 0.07 St (1 Stokes = 10^{-4} m^2 s^{-1}) the density-normalized complex elastic parameters are A_{11} = (5.28, 0.223), A_{22} = (8.59, 0.025), A_{44} = (3.0, 0.0), A_{55} = (2.39, 0.0), and A_{12} = (1.76, 0.074). For smaller values of kinematic viscosity the magnitude of the imaginary parts decreases. For kinematic viscosities 0.04 and 0.01, the latter corresponds to water, the complex elastic parameters are A_{11} = (5.28, 0.127), A_{22} = (8.59, 0.014) and A_{12} = (1.76, 0.043), and A_{11} = (5.28, 0.032), A_{22} = (8.59, 0.004) and A_{12} = (1.76, 0.011), respectively. The real parts of elastic parameters and, therefore, velocity anisotropy, do not depend on the viscosity as long as the conditions of applicability of Hudson's (1988) theory are not violated.

The magnitude of the imaginary parts of elastic parameters is mainly controlled by the kinematic viscosity of the liquid, the degree of saturation of the cracks, the frequency of the penetrating waves and the crack aspect ratio (for more details, see Hudson, 1988). The imaginary parts of elastic parameters of the above described models are relatively large (see, e.g., the ratio of imaginary to real part for A_{11} which is 0.042 for a kinematic viscosity of 0.07 St) nevertheless, the calculated Q values (equation 7) for the considered profile directions and wave types are far above 50 for all numerical examples presented in this paper.

Additional attenuation can be caused by scattering of waves on cracks. According to Hudson (1990), however, "for crack radii and crack spacing small compared with the wavelength," which is the case considered in this paper, "the effective material parameters contain no attenuation component arising from scattering (only higher order terms account for attenuation due to scattering)." Therefore, attenuation due to scattering is not considered in this paper.

Three-component receivers are located in the vertical borehole in the depth range from 0.5 to 2.0 km with 50-m spacing. The receivers are oriented as follows: the vertical component is positive upward, the radial component is oriented along the line connecting the source and the mouth of the borehole, positive away from the source, and the transverse component is oriented so that the system is right-handed.

Single force point sources of unit strength are located at the free surface (the effects of the free surface at the source are not considered). Three different orientations of single forces are used: vertical force pointing downward, radial force along the line connecting the source and the mouth of the borehole, pointing towards the borehole, and transverse force perpendicular to the previous two forces and oriented so that all three forces form a right-handed system. As a source time function, the Gaussian envelope signal (Červený et al., 1977) with a prevailing frequency of 50 Hz and $\gamma = 4$ is used. No phase or time shift is applied, so that the signal is cosine shaped and its arrival time corresponds to the

maximum amplitude of the envelope of the signal (zero phase wavelet).

All direct waves and all primary reflected unconverted waves are considered. We consider as converted only those waves which transform at an interface from compressional (quasi-compressional) to shear (quasi-shear) waves or vice-versa (the transformation from one qS-wave to the other is not considered a conversion). The waves propagating only in isotropic layers are denoted by P or S, the waves propagating, at least partially, in the anisotropic layer are denoted by qP, $qS1$, and $qS2$ ($qS1$ corresponds to the faster propagating quasi-shear wave, $qS2$ corresponds to the slower propagating quasi-shear wave). Direct waves are denoted by a subscript d. The integer subscript in the name of the wave indicates the number of the interface where the wave is reflected. In this way, for example, $qS2_3$ denotes the slower quasi-shear wave reflected at the interface 3.

VSP COMPUTATIONS

The geometry of the VSP experiment is schematically shown in Figure 5. The coordinates of the mouth of the vertical borehole are x = 2.5 km and y = 2.3 km. Two locations of point sources at the free surface are considered. Their coordinates are x = 2.5 km, y = 1.3 km, and x = 3.2 km, y = 1.6 km, respectively. The two locations of sources define two source-borehole profiles with azimuths 90 degrees and 135 degrees measured from the positive x-axis. The 90-degree profile runs along the strike of cracks, the 135-degree runs 45 degrees off the strike of cracks.

Frequency Responses and Selected VSP Synthetics

In this section frequency responses and selected synthetic seismograms for different values of kinematic viscosity of the pore fluid resulting in different attenuation behavior are

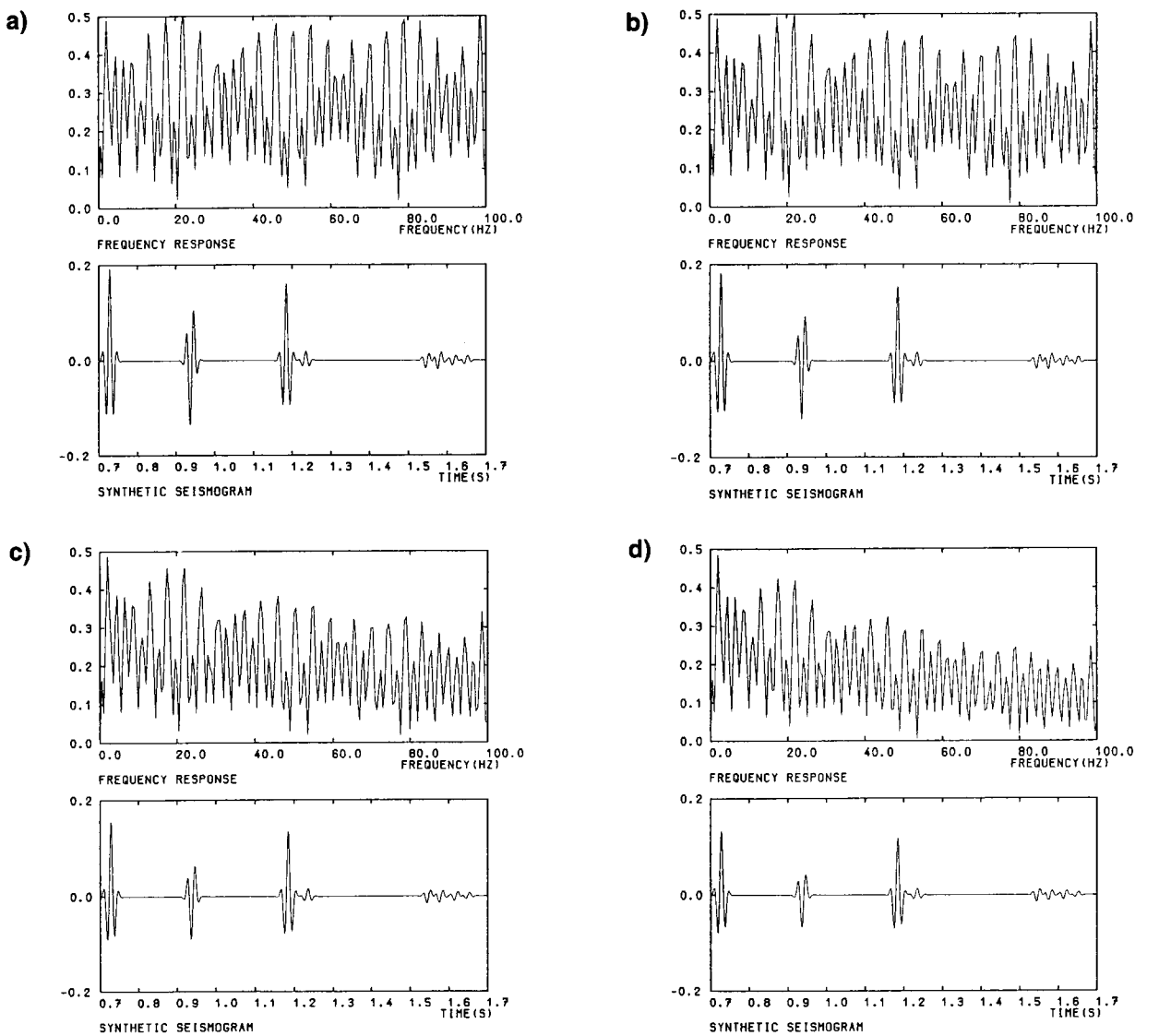

FIG. 6. Frequency responses (top) and synthetic seismograms (bottom) of the vertical component of the displacement vector generated by a vertical force and recorded at the receiver at 1.6 km depth. Perfectly elastic anisotropic model (a), attenuating anisotropic model with partially liquid saturated aligned cracks (saturation = 70 percent) where the kinematic viscosities of the pore fluid are 0.01, i.e., water (b), 0.04 (c), and 0.07 St (d).

discussed. Frequency responses and synthetic seismograms of the vertical component of the displacement vector, generated by vertical force on the profile 135 degrees are shown in Figure 6. The receiver is situated at 1.6 km depth, i.e., in the anisotropic layer. Four different situations are considered: a perfectly elastic model, considering only the velocity anisotropy caused by dry aligned cracks (Figure 6a), and attenuating models of partially saturated (70 percent) aligned cracks, where the values of kinematic viscosity of the pore fluids are 0.01 (water), 0.04, and 0.07 St, respectively (Figures 6b-d). The upper frames show the frequency responses, the bottom frames show synthetic seismograms. With increasing attenuation, i.e., with increasing kinematic viscosity, the frequency responses decrease faster with increasing frequency.

Individual phases appearing in synthetic seismograms of Figures 6a-d are as follows (from left to right): qP_d, qP_3, $qS1_d$, $qS2_d$. The arrivals between 1.5 and 1.7 s consist successively of four arriving waves: $qS1_3$ wave, waves transformed from $qS1$ to $qS2$ and vice versa during the reflection at interface 3, and $qS2_3$ wave. It is of interest to note that the transformed phases are as strong as or even stronger than $qS1_3$ or $qS2_3$ phases. Comparison of synthetic seismograms in Figures 6a-d shows that all waves are affected by attenuation. Comparing Figure 6d (kinematic viscosity of 0.07 St) with the perfect elastic case (Figure 6a) the qP_d phase is about 30-percent weaker in the attenuated case. Also a change in phase can be detected. For the qP_3 phase the decrease in amplitude is more than 50 percent, which expresses the dependence of Q on the propagation direction in anisotropic attenuating media. The $qS1_d$ and $qS2_d$ amplitudes are attenuated similarly and are about 27 percent weaker in the attenuated case (Figure 6d) than in the perfect elastic case (Figure 6a). For the quasi S-wave reflections the faster propagating $qS1_3$ phase is less attenuated (15 percent) than the slower propagating $qS2_3$ phase (about 40 percent). The feature, that quasi S-waves can be attenuated differently, is called differential attenuation (Crampin, 1989).

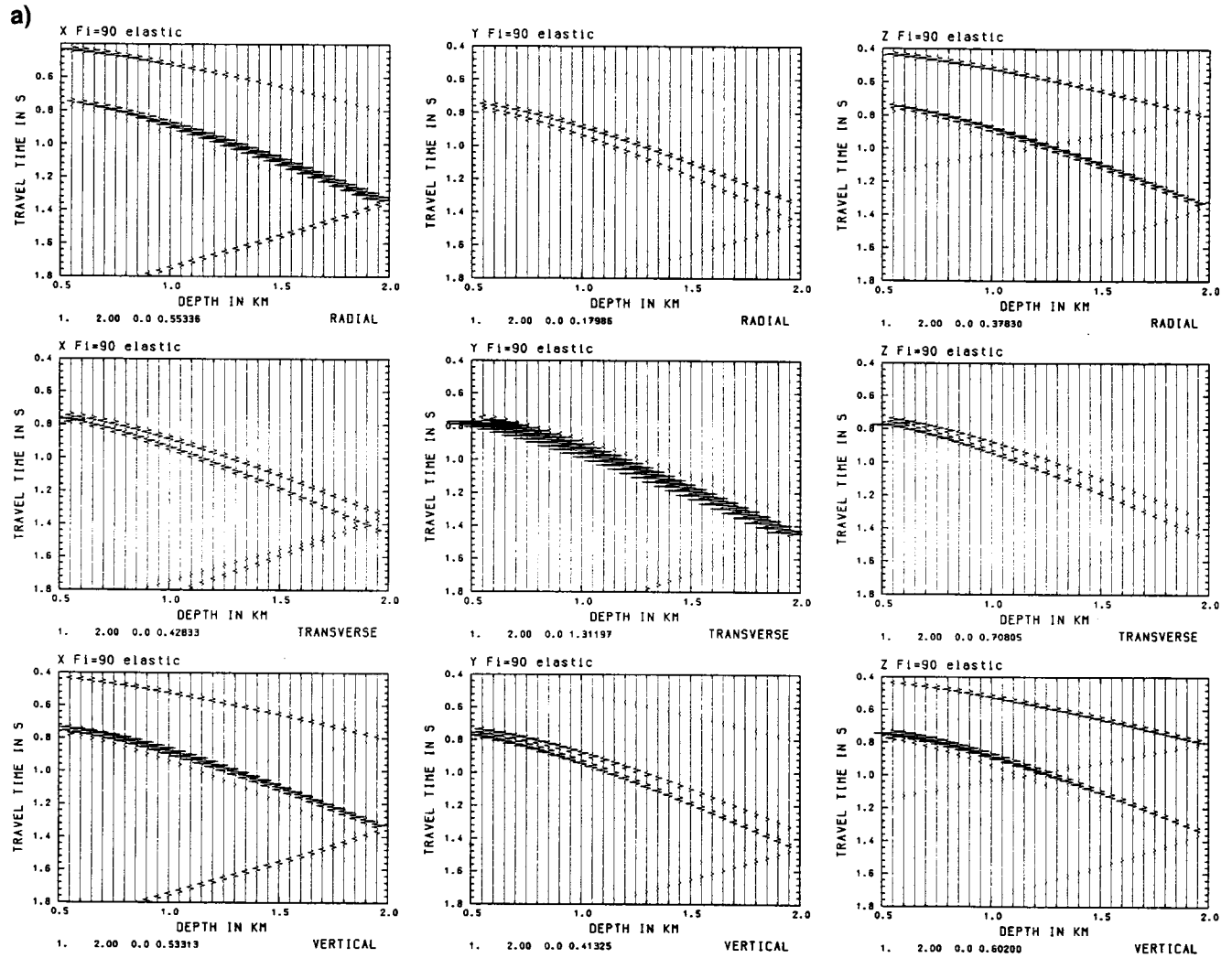

FIG. 7. Multisource three-component VSP synthetics observed for the azimuth of 90 degrees. (a) Perfect elastic anisotropic model and (b) attenuating anisotropic model based on partially liquid saturated aligned cracks (saturation = 70 percent), where the kinematic viscosity of the pore fluid is 0.07 St. Columns from left to right correspond to radial, transverse, and vertical single force; the lines from top to bottom correspond to radial, transverse, and vertical component of the displacement vector.

Nine-Component VSP Synthetics

In this section synthetic vector wavefields for the anisotropic attenuating model described above are presented in the form of nine-component VSP synthetics. The results for the attenuating model with a kinematic viscosity of 0.07 St (strongest considered attenuation) are compared with those for the perfectly elastic model (with the same velocity anisotropy) to show the effects of attenuation on the wavefield.

For receivers deeper than 1.3 km the sequence of arrivals is (from top to bottom, i.e., with increasing traveltime): qP_d, qP_3, $qS1_d$, $qS2_d$, and the group of four reflected arrivals starting with $qS1_3$ and ending with $qS2_3$ phase. For the shallower receivers, the above sequence of arrivals changes so that the qP_3 reflection arrives later than the $qS1_d$ and $qS2_d$ phases.

In Figures 7 and 8, nine-component synthetic seismograms are shown. Each set of seismograms is organized so that columns from left to right correspond to radial, transverse, and vertical single-force point sources. The upper frames correspond to radial, middle to transverse, and lower to vertical components of the displacement vector. No amplitude power scaling is used, true amplitudes are presented.

In Figure 7, the VSP synthetics observed along the profile with azimuth of 90 degrees, i.e., along the strike of the cracks, are shown. Figure 7a shows results for the perfectly elastic anisotropic model, whereas Figure 7b shows the synthetics for the attenuating anisotropic model. For this azimuth almost no differences between the perfectly elastic model and the attenuating model are visible. Due to the orientation of the profile, phases transformed from $qS1$ wave to $qS2$ and vice versa during the reflection at inter face 3 are practically invisible. Inspection of single traces with larger amplitude scaling (not reproduced here) reveals that quasi-S-waves are more affected than quasi-P-waves and that the slower propagating quasi-S waves are more strongly attenuated than the faster quasi-S-waves. However, the total reduction in amplitude is only a few percent. For this particular profile the attenuating effects of partial liquid saturation of aligned cracks are practically negligible.

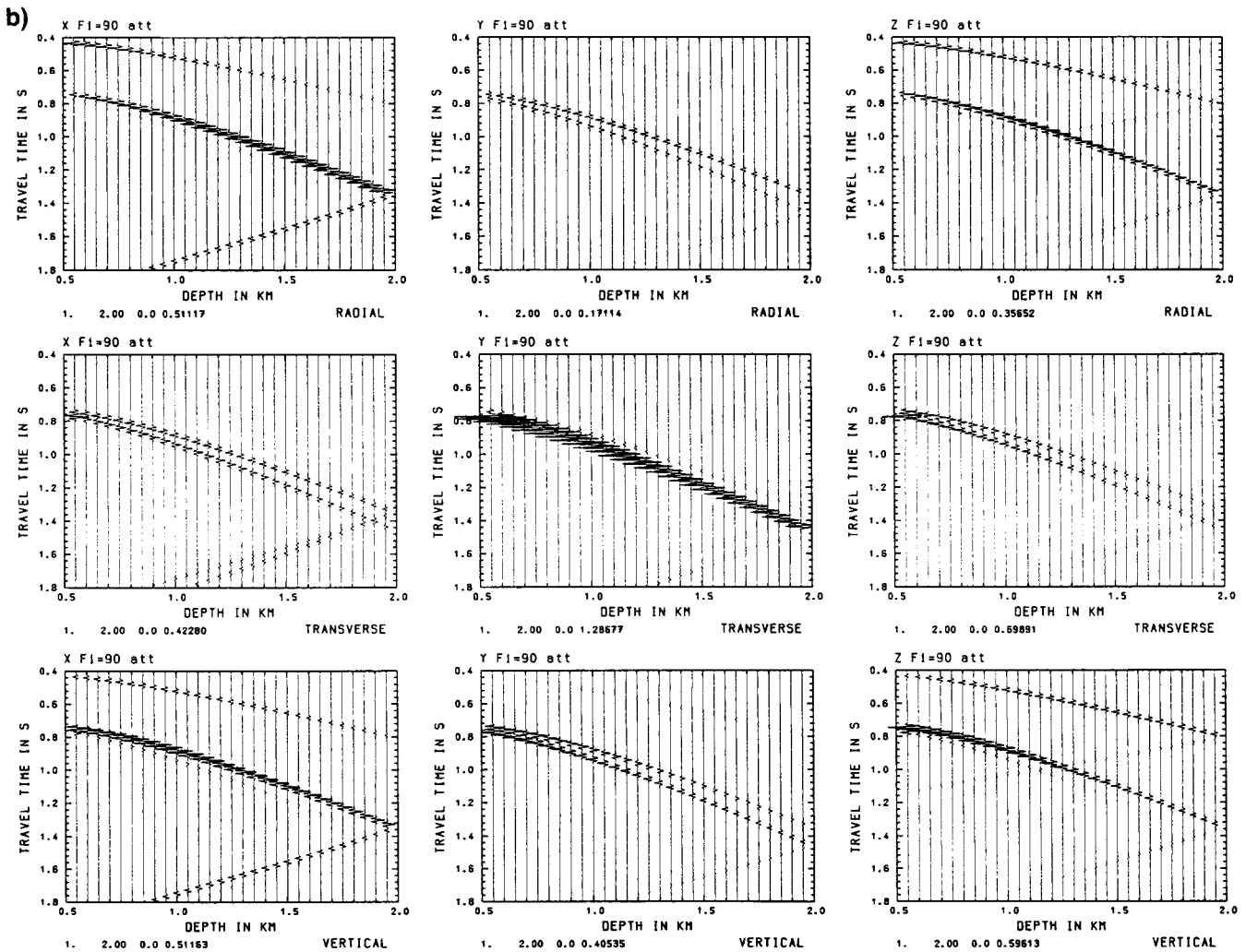

FIG. 7. (continued)

Figure 8 shows the vector wavefield recorded along the profile with azimuth of 135 degrees, i.e., 45 degrees off strike of cracks. Figure 8a shows the elastic case and Figure 8b the attenuating model. For this profile direction the effects of partial liquid saturation of aligned cracks are clearly visible in the seismograms. Amplitudes of all phases are affected. The longer the raypath in the attenuating layer the larger is the amplitude decay. The phases recorded at receivers situated at greater depths are, therefore, more strongly attenuated. Besides the effects caused by attenuation, the sections in Figure 8 show another interesting feature for the direct quasi-S-wave. The amplitudes of the $qS1_d$ and the $qS2_d$ phases strongly vary with the receiver depth (e.g., see the transverse components for the vertical and radial forces or the radial and vertical components for the transverse force for receivers from 0.6 to 0.8 km depth). The way in which all the three components of these phases vary indicates twisting of the polarization vectors with depth. Since the layer in which the twisting of polarization vectors occurs is homogeneous, anisotropy is fully responsible for the variation of the polarization. For the profile with an azimuth of 90 degrees (Figure 7), which is almost a symmetry plane (but note that cracks dip by 70 degrees), such twisting is not observed.

DISCUSSION

The interest in the effects of attenuation on seismic wave propagation in anisotropic media will increase, mainly in connection with crack-induced anisotropy. Because of its directional dependence, attenuation in anisotropic media represents a valuable additional constraint to construct the model of the investigated structure.

To incorporate attenuation effects into ray computations, we used the so-called weak attenuation concept. This approach allows us to use real rays instead of complex rays, which should be used in attenuating structures. On the other hand, the approach is approximate and it is supposed to work well only for sufficiently large values of quality factor. Comparison of ray computations with results of the reflectivity method shows, however, that the weak attenuation concept can be applied to a quite broad range of realistic values of quality factor in the experiment configurations

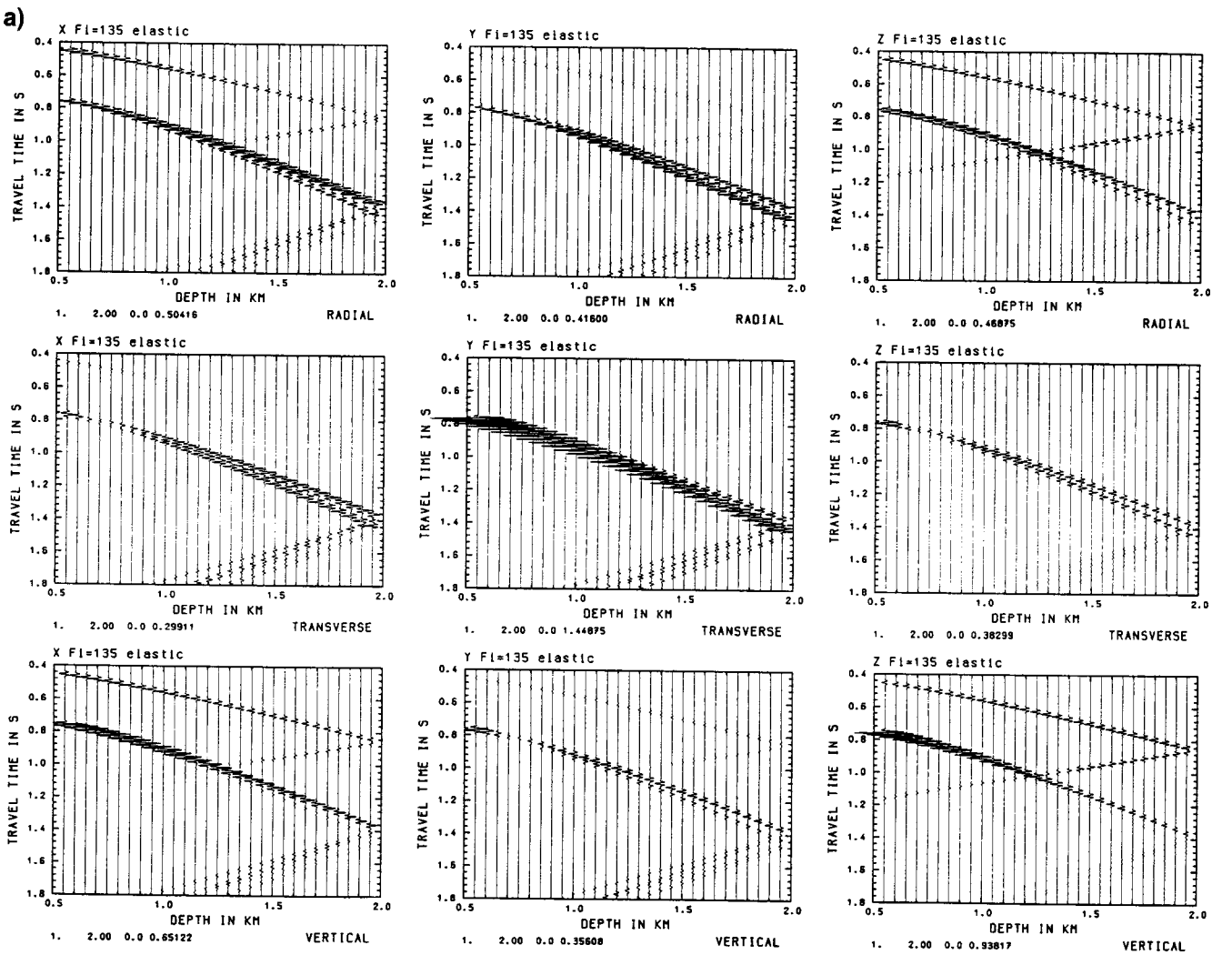

FIG. 8. The same as Figure 7, but for an azimuth of 135 degrees.

comparable with that considered in this paper. For signals with prevailing frequency of about 33 Hz, the comparison has shown that the concept is applicable to media with quality factor as low as $Q = 50$; i.e., it is applicable even for models of attenuating sediments. In terms of imaginary parts of group velocity this means that the imaginary parts should be 100 times less than the real parts or smaller. This criterion can be simply incorporated into the program and checked during the computations.

In the examples considered, the weak attenuation concept allowed the computations to be performed on the CONVEX C1 computer practically as fast as for perfectly elastic anisotropic media. About 5 percent more CPU time was needed for noncausal absorption computations [see discussion after equations (9) and (10)] and about 10 percent more CPU time for causal absorption compared with the computations for the perfectly elastic case. The computation speed for anisotropic media with causal absorption can be increased by linearization of equation (9), see Červený and Frangié (1982). The CPU time for the computation of nine-component vector wavefields with causal absorption shown in Figures 7b and 8b was about 210 s each.

The quality factor in an anisotropic attenuating model is quantity, which generally depends on the orientation of the wave normal and on the polarization of the considered wave (see equation 7). Due to this, different waves are affected in a different way. For example, in the presented results, the slower propagating reflected quasi shear-wave was more affected than the faster one. This effect is called differential attenuation. Attenuation anisotropy could be also used as an additional parameter to the velocity anisotropy in the repeated experiments monitoring changes in the crack aspect ratio (Douma and Crampin, 1990), as the attenuation of partially liquid saturated aligned cracks depends on the crack aspect ratio.

The material of the pore space as well as the degree of saturation and the shape of the pores have an effect on the attenuation of the medium. Changes in these parameters result in an alteration of the attenuating behavior of the medium. Crampin (1989) suggests using these effects to monitor changes of the saturation and the viscosity of the pore space material during the production of an oil field by repeated VSP experiments.

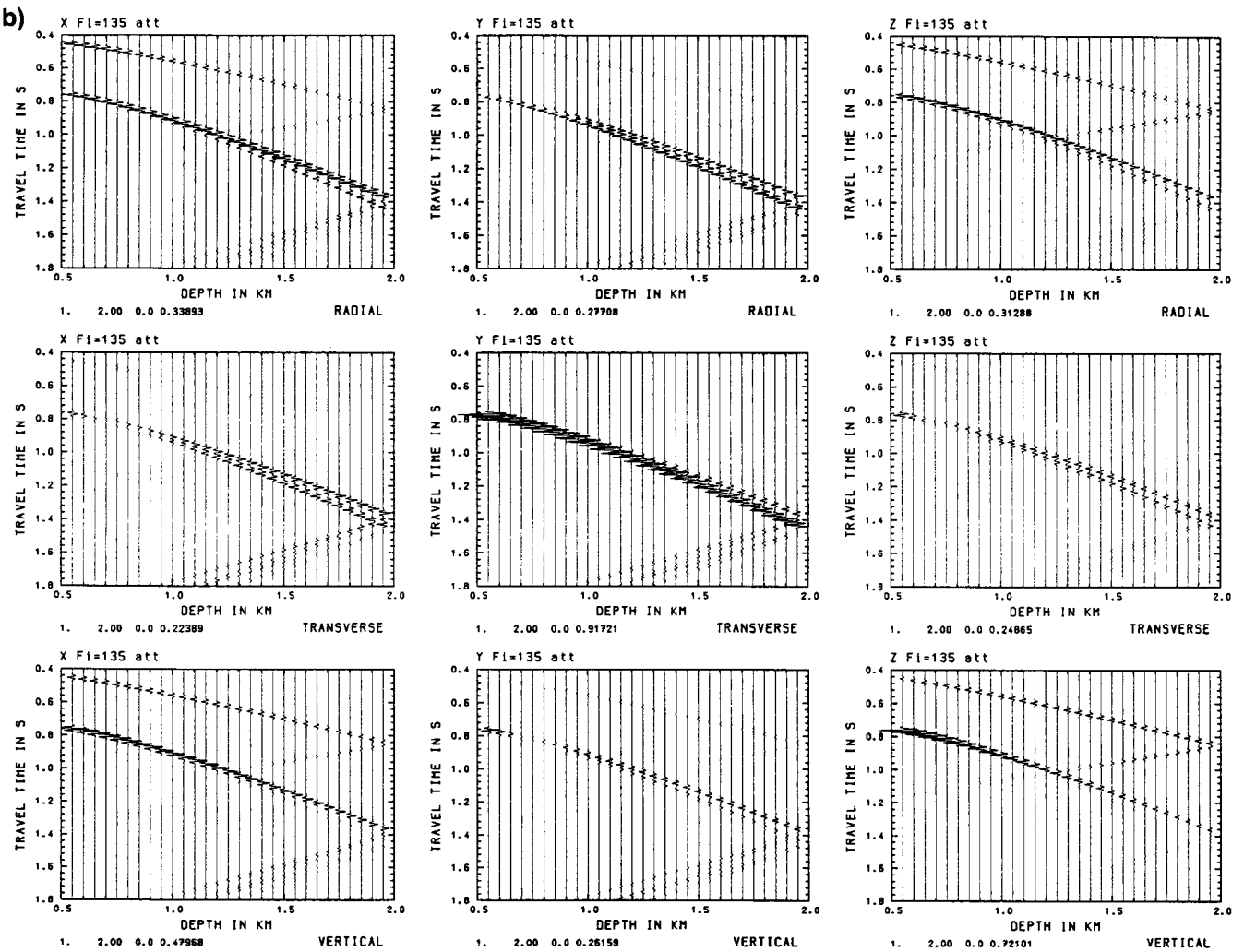

FIG. 8. (continued)

We believe that the results of this paper also show the importance of recording vector wavefields to investigate the earth's crust, especially its anisotropy. The energy distribution into different components, i.e., the orientation of polarization vectors, which can only be derived from the complete vector wavefield, yield important constraints on the form of the model.

ACKNOWLEDGMENTS

We are grateful to T. McEvilly and E. Majer for enabling us to carry out this study at the Center for Computational Seismology (CCS), Lawrence Berkeley Laboratory, Berkeley. Computations were performed on the CONVEX C1 computer of CCS and the IBM 3090 of the Computer Center of the University of Clausthal. We are grateful to V. Červený for allowing us to use and modify programs from the BEAM87 package and thank him for a critical reading of the manuscript. A thorough review by Dennis Corrigan and an unknown reviewer is appreciated. This work was partially supported by the director, office of Civilian Radioactive Waste Management, office of Facilities Siting and Development, Siting and Facilities Technology Division of the U.S. Department of Energy under contract #DE-AC03-76SF00098. D.G. was also supported by a grant from the German Research Society (DFG grant III 02-GA 350/1-1).

REFERENCES

Červený, V., 1982, Direct and inverse kinematic problems for inhomogeneous anisotropic media: Contr. Geophys. Inst. Slov. Acad. Sci., **13**, 127–133.

——— 1985, Ray synthetic seismograms for complex two-dimensional and three-dimensional structures: J. Geophys., **58**, 2–26.

Červený, V., and Frangié, A. B., 1982, Effects of causal absorption on seismic body waves: Studia geophys. geod., **26**, 238–253.

Červený, V., Molotkov, I. A., and Pšenčík, I., 1977, Ray method in seismology: Charles University Press.

Červený, V., and Pšenčík, I., 1984, SEIS83—Numerical modeling of seismic wave fields in 2-D laterally varying layered structures by the ray method, *in* Engdahl, E. R., Ed., Documentation of earthquake algorithms, Report SE-35: World Data Center (A) for Solid Earth Geophysics. 36–40.

——— 1988, Synthetic body wave seismograms for slightly dissipative laterally varying crustal models, *in* Nersesov, L. N., Ed., Recent seismological investigations in Europe: Nauka, 530–537.

Crampin, S., 1984, Effective elastic constants for wave propagation through cracked solids: Geophys. J. R. Astron. Soc., **76**, 17–28.

——— 1985, Evidence for aligned cracks in the earth's crust: First Break, **3**, no. 3, 12–15.

——— 1987, Geological and industrial implications of extensive-dilatancy anisotropy: Nature, **328**, 491–496.

——— 1989, The future in production engineering: Abstracts conf. rec. proc. vector wavefield data: Soc. Expl. Geophys., 126.

——— 1990, Alignment of near-surface inclusions and appropriate crack geometries for geothermal hot-dry-rock experiments: Geophys. Prosp., **38**, 621–631.

Crampin, S., Bush, I., Naville, C., and Taylor, D. B., 1986, Estimating the internal structure of reservoirs with shear-wave VSPs: The Leading Edge, **5**, 35–39.

Crampin, S., Lynn, H. B., and Booth, D. C., 1989, Shear-wave VSPs: A powerful new tool for fracture and reservoir description: J Petr. Tech., **5**, 283–288.

Douma, J., and Crampin, S., 1990, The effect of a changing aspect ratio of aligned cracks on shear-wave vertical seismic profiles: A theoretical study: J. Geophys. Res., **95**, 11293–11300.

Fuchs, K., and Müller, G., 1971, Computation of synthetic seismograms with the reflectivity method and comparison with observations: Geophys. J. Roy. Astr. Soc., **23**, 417–433.

Futterman, W. I., 1962, Dispersive body waves: J. Geophys. Res., **67**, 5279–5291.

Gajewski, D., and Pšenčík, I., 1987, Computation of high-frequency seismic wavefields in 3-D laterally inhomogeneous anisotropic media: Geophys. J. Roy. Astr. Soc., **91**, 383–411.

——— 1990, Vertical seismic profile synthetics by dynamic ray tracing in laterally varying layered anisotropic structures: J. Geophys. Res., **95**, 11301–11316.

Hanyga, A., 1982, The kinematic inverse problem for weakly laterally inhomogeneous anisotropic media: Tectonophysics, **90**, 253–262.

Hudson, J. A., 1981, Wave speeds and attenuation of elastic waves in material containing cracks: Geophys. J. Roy. Astr. Soc., **64**, 133–150.

——— 1988, Seismic wave propagation through material containing partially saturated cracks: Geophys. J., **92**, 33–37.

——— 1990, Attenuation due to second order scattering in material containing cracks: Geophys. J. Internat., **102**, 485–490.

Jech, J., and Pšenčík, I., 1989, First-order perturbation method for anisotropic media: Geophys. J. Internat., **99**, 369–376.

Kjartansson, E., 1979, Constant Q wave propagation and attenuation: J. Geophys. Res., **84**, 4737–4748.

Kravtsov, Yu. A., and Orlov, Yu. I., 1990, Geometrical optics of inhomogeneous media: Springer Verlag New York, Inc.

Mavko, G. M., and Nur, A., 1979, Wave attenuation in partially saturated rocks: Geophysics, **44**, 161–178.

Moczo, P., Bard, P.-Y., and Pšenčík, I., 1987, Seismic response of two-dimensional absorbing structures by the ray method: J. Geophys., **62**, 38–49.

Müller, G., 1983, Rheological properties and velocity dispersion of a medium with power-law dependence of Q on frequency: J. Geophys., **54**, 20–29.

O'Connell, R. J., and Budiansky, B., 1977, Viscoelastic properties of fluid-saturated cracked solids: J. Geophys. Res., **82**, 5719–5735.

Sandmeier, K.-J., 1984, Modification and extension of the reflectivity program to compute synthetic seismograms (in German): Diploma Thesis, University of Karlsruhe.